JACS
JOURNAL OF THE AMERICAN CHEMICAL SOCIETY
Article
pubs.acs.org/JACS

Precise and Reversible Protein-Microtubule-Like Structure with Helicity Driven by Dual Supramolecular Interactions

Guang Yang,[†] Xiang Zhang,[‡] Zdravko Kochovski,[§,∥] Yufei Zhang,[†] Bin Dai,[‡] Fuji Sakai,[†] Lin Jiang,[⊥] Yan Lu,[§] Matthias Ballauff,[§] Xueming Li,[#] Cong Liu,[*,‡] Guosong Chen,[*,†] and Ming Jiang[†]

[†]The State Key Laboratory of Molecular Engineering of Polymers and Department of Macromolecular Science, Fudan University, Shanghai 200433, China

[§]Soft Matter and Functional Materials, Helmholtz-Zentrum Berlin für Materialien und Energie, 14109 Berlin, Germany

[‡]Interdisciplinary Research Center on Biology and Chemistry, Shanghai Institute of Organic Chemistry, Chinese Academy of Sciences, Shanghai 200032, China

[∥]TEM Group, Institute of Physics, Humboldt-Universität zu Berlin, 12489 Berlin, Germany

[⊥]Department of Neurology, Easton Center for Alzheimer's Disease Research, David Geffen School of Medicine, University of California, Los Angeles, California 90095, United States

[#]Ministry of Education Key Laboratory of Protein Science, Center for Structural Biology, Tsinghua-Peking Joint Center for Life Sciences, School of Life Sciences, Tsinghua University, Beijing 100084, China

Supporting Information

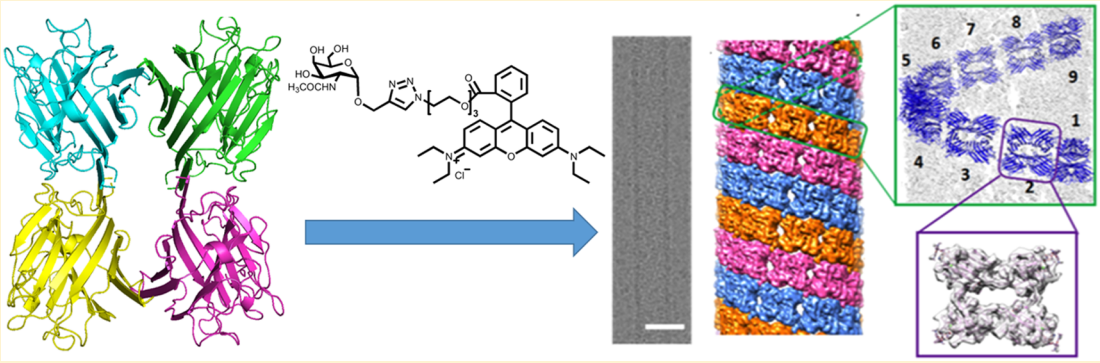

ABSTRACT: Protein microtubule is a significant self-assembled architecture found in nature with crucial biological functions. However, mimicking protein microtubules with precise structure and controllable self-assembly behavior remains highly challenging. In this work, we demonstrate that by using dual supramolecular interactions from a series of well-designed ligands, i.e., protein−sugar interaction and $\pi-\pi$ stacking, highly homogeneous protein microtubes were achieved from tetrameric soybean agglutinin without any chemical or biological modification. Using combined cryo-EM single-particle reconstruction and computational modeling, the accurate structure of protein microtube was determined. The helical protein microtube is consisted of three protofilaments, each of which features an array of soybean agglutinin tetramer linked by the designed ligands. Notably, the microtubes resemble the natural microtubules in their structural and dynamic features such as the shape and diameter and the controllable and reversible assembly behavior, among others. Furthermore, the protein microtubes showed an ability to enhance immune response, demonstrating its great potential for biological applications.

INTRODUCTION

Protein self-assembly affords a series of unique functional opportunities ranging from the dynamic cellular scaffolding provided by the cytoskeletal proteins to encapsulation, protection, and delivery of viral genomes to new host cells by virus capsids.[1] The beauty of the self-assembled architectures with diverse biological functions has inspired studies on the development of novel nanostructures formed by designed proteins.[2−8] Until now, a variety of artificial protein nanostructures including cages, filaments, nanosheets, and crystals has been successfully constructed in zero (0D), one (1D), two (2D), and three dimensions (3D).[9−16]

Among different architectures, tubular structure is particularly interesting and of great importance, as demonstrated by the most well-known protein tubular structure found in nature, i.e., microtubules. As one of the key components of the cytoskeleton, microtubule is characterized as a long, filamentous, and tube-shaped self-assembled protein architecture

Received: November 9, 2015
Published: January 22, 2016

 © 2016 American Chemical Society
DOI: 10.1021/jacs.5b11733
J. Am. Chem. Soc. 2016, 138, 1932−1937

essential in all eukaryotic cells.[17] The microtubule features include precise packing of proteins and dynamic association and dissociation, among others, and they are considered one of the most typical examples of supramolecular structures in nature.[18] Although the natural tubular structure attracts a broad interest of both chemists and biologists, until now successful artificial mircotubular structures are rare in the literature because of the complexity of their formation process,[19,20] and most of them were constructed by oligopeptides,[21,22] DNA,[23,24] and rod-coiled organic molecules.[25−27] The few reported protein microtubes were prepared in laboratories exclusively from either ring-shaped proteins[28−30] or tubulin. Besides, only metal−ligand interaction was employed to construct mutant proteins into tubes, in which strong protein−protein interaction also played an important role.[3,20,31] However, none of them possess a precise and reversible self-assembled structure as the natural microtubule does.

In short, protein microtubular structures constructed by supramolecular interactions from natural proteins have not been reported so far. In this work, we designed and achieved the self-assembled protein-microtubule-like structure by dual weak supramolecular interactions rather than protein−protein interactions. This has been clearly demonstrated by the cryo-electron microscopy (Cryo-EM) studies of the resultant microtubes with a resolution of 7.9 Å by single-particle analysis. From the structure and further study, we found that the protein microtube was formed by the processes of protofilament growth and twisting driven by the dual noncovalent interactions between neighboring proteins in the same protofilament. This feature renders the tube a precise self-assembled structure, very similar to that of microtubules in nature, which makes it unique to all of the reported protein micro- or nanotubes. Furthermore, similar to the dynamic nature of microtubules, our microtubule-like structure can be controlled thermodynamically and kinetically, and its dissociation and formation can be tuned by supramolecular means as well.

■ RESULT AND DISCUSSION

Design of the Protein Building Block and Noncovalent Interactions. In our previous study, we reported that a 3D crystalline framework (PCF) was constructed from lectin concanavalin A (Con A), via a combination of Con A/α-mannopyanoside (α-Man) interaction and π−π stacking of Rhodamine B (RhB),[32] where the functional species existed in the introduced ligands. In the study, PCF instead of the desired microtubule-like structure was produced, probably because of the tetrahedral structure of ConA, which tends to form a 3D frame. In the current study, targeting at a protein-microtubule-like architecture, soybean agglutinin (SBA) was selected as a building block that was a homotetrameric protein exhibiting D2 symmetry with a nearly planar shape and that did not form any tubular structures itself in nature. The tetrameric SBA contains four identical sugar-binding sites, which can specifically capture *N*-acetyl-α-D-galactosamine (GalNAc) or α-D-galactopyranoside (Gal) in the presence of Ca^{2+} and Mn^{2+}.[33] As shown in Figure 1a, the four sugar-binding sites of SBA are not on the same plane, which avoids the formation of 1D fibrillar structure. Four ligands of small molecules, **R3GN** and **RnG** (n = 2, 3, and 4) were designed and synthesized to induce the self-assembly of SBA (Figure 1b). The ligands are composed of three moieties including (1) a sugar unit of GalNAc or Gal, which is capable of binding to SBA,[34] (2) Rhodamine B (RhB), which was responsible for possible ligand dimerization due to π−π stacking, and (3) a short oligo(ethylene oxide) spacer of varying length linking the sugar and RhB. As controls, **R3M** with α-D-mannopyranoside (Man) replacing GalNAc and E3GN with GalNAc but without RhB were also synthesized. The synthesis details and characterization of compounds **R3GN**, **RnG** (n = 2, 3, and 4), **R3M**, and **E3GN** are shown in Scheme S1. The designed **E3GN** binds tightly to SBA with the binding constant of 4.47×10^4 M^{-2} at 20 °C (Figure S1) measured by isothermal titration calorimetry (ITC), which was similar to the reported results.[34]

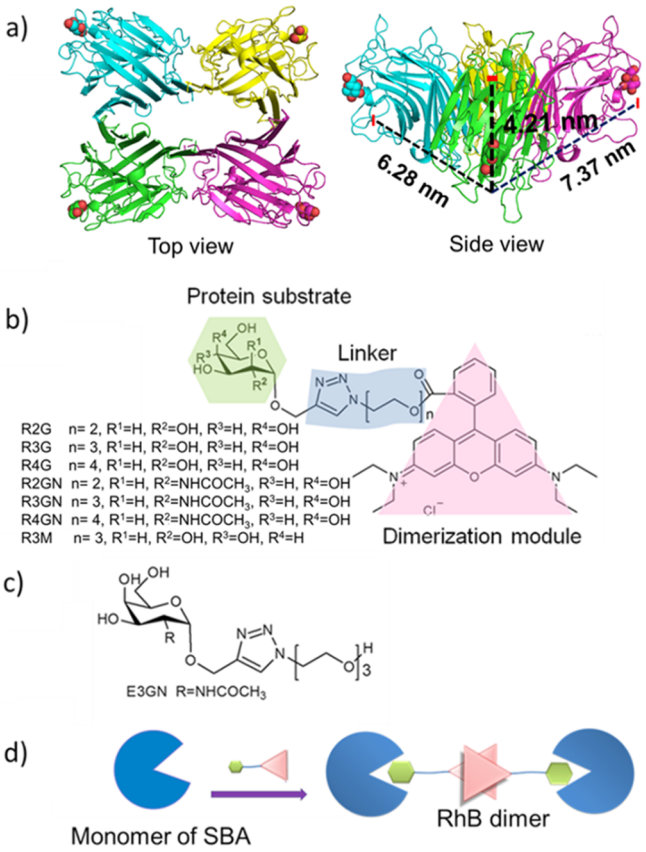

Figure 1. (a) Shape and size of SBA tetramer. The filled space model represents the GalNAc binding on the protein (structure adapted from reported crystal structure, Protein Databank accession code: 1SBE). Chemical structures of (b) the inducing ligands and (c) **E3GN**. (d) Interactions between SBA monomer and GalNAc or Gal and RhB dimerization after being tethered to SBA.

Preparation and Characterization of the Protein Microtube. Protein microtubes were achieved in solution by incubating tetrameric SBA (0.2 mM) in the presence of **R3GN** at 4 °C. Typically, equimolar quantities of **R3GN** were added to SBA in 4-(2-hydroxyethyl)-1-piperazineethanesulfonic acid (HEPES) buffer ([HEPES] = 20 mM, [NaCl] = 40 mM, [$CaCl_2$] = 5 mM, and [$MnCl_2$] = 5 mM); the final concentration of **R3GN** and SBA monomer was 0.2 mM. After the two components were mixed together and kept at 4 °C over 72 h, no precipitates were observed. However, dynamic light scattering (DLS) results indicated formation of self-assembled structures in the solution (Figure S2). Under cryo-EM, highly homogeneous microtubular structures were observed with a micrometer-scale length and a width of around 26 nm (Figures 2a,b and S3). The hollow structure is confirmed by the obvious contrast between the outer and inner parts in all of the observed assemblies.

DOI: 10.1021/jacs.5b11733
J. Am. Chem. Soc. 2016, 138, 1932−1937

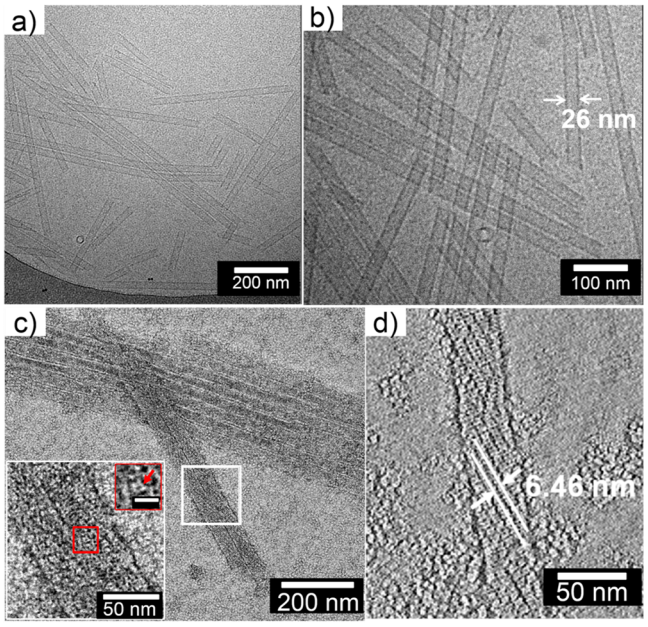

Figure 2. (a and b) Protein microtubes visualized by Cryo-EM at different magnifications. (c) EM micrograph of negatively stained protein microtubes. Insets: enlarged versions of marked areas, scale bar: 10 nm. (d) Slice (0.8 nm thick, *xy*) through the 3D tomographic reconstruction of negatively stained protein microtubes.

The tubular structure was also confirmed by cryo-electron tomography (Cryo-ET), as shown in (Figure S4). The diameter of the protein microtube was measured as around 26 nm in Cryo-EM micrographs, whereas 36 ± 2 nm was found in electron micrographs of negatively stained samples (Figure S5a,b). Considering the well-preserved tubular structure under cryo-EM and the dehydration and collapse of the hollow structure under the negative-stain EM, the two values seemed quite consistent, i.e., the perimeter of the microtube found under cryo-EM is equal to twice of that observed under negative-stain EM: $(26 \times \pi)/2 \approx 40.8$ nm. This means that the microtubes were collapsed into ribbons under the negative-stain EM. The collapsed microtube can also be observed directly by 3D tomographic reconstructions of the negatively stained microtubes (Figure S6). As shown in Figure S5c,d, atomic force microscopy (AFM) gave the height of the collapsed microtubes of around 9.4 nm uniformly. This height was very close to that of a superposition of two layers of SBA (thickness of a tetramer protein of about 4.2 nm, Figure 1a), indicating that the microtube wall was a monolayer of tetrameric SBA. Negative-stain EM revealed more structural information in detail. As shown in the inset of Figure 2c, the white ring represents a single SBA tetramer, which packed regularly into quadrangles within the microtube. Then, an *xy* slice through a 3D tomographic reconstruction of the negatively stained microtubes shown in Figure 2d further proved its collapsed state under drying and, particularly, some periodic packing with a helical structure within the tube wall (Figure S6), and the helical protofilament periodicity was determined as 6.46 nm (Figure 2d). Small-angle X-ray scattering (SAXS) results gave the distance between two protofilaments was about 6.4 nm (Figure S7), which was consistent with the 3D tomographic reconstruction result. In addition, some long microtubes with a length reaching a micrometer scale show a slight curvature under cryo-EM and negative-stain EM (Figure S8), which is understandable because generally flexibility of linear materials could be induced when the ratio of length to diameter reaches a certain value. Interestingly, all of other designed ligands, **R2G**, **R3G**, and **R4G** with Gal replacing GalNAc with different spacer lengths, are capable of inducing formation of SBA protein microtubes with indistinguishable morphology and uniform width, the same as that formed by SBA/**R3GN** under cryo-EM (Figure S9).

Cryo-EM 3D Reconstruction and Computational Modeling. To elucidate how tetrameric SBA self-assembles into tubular structure mediated by the designed ligands, the structure of the microtubes of SBA and **R3GN** was studied in detail by cryo-EM 3D reconstruction at around 7.9 Å resolution (Figures 3 and S10). The 3D reconstruction result not only

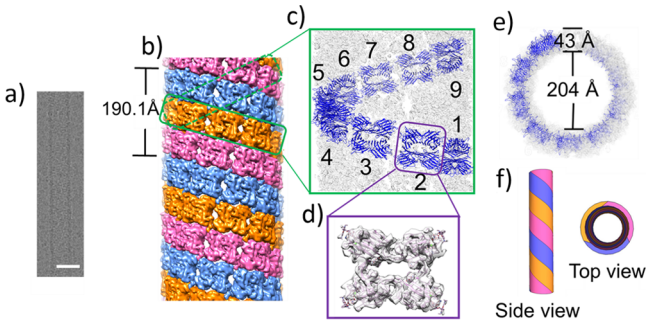

Figure 3. Structural model of SBA microtube. (a) Single SBA microtube visualized by Cryo-EM (Scale bar: 25 nm). (b) Electron density map of SBA microtube after 3D reconstruction. Three neighboring protofilaments are respectively colored in red, yellow, and blue. The length of each turn (periodicity) is ∼19 nm. (c) Each turn is composed of nine identical tetrameric SBA molecules colored in blue. (d) Tetrameric SBA model fitted in the electron density map. (e) Top view of microtube model. The thickness of the tube wall is ∼4 nm. The inner diameter of the microtube is ∼20 nm. Each SBA tetramer in one periodic helical structure is shown in blue in c and e. (f) Cartoon model of the microtube. The three protofilaments are colored in red, yellow, and blue, respectively.

demonstrates the tubular architecture but also reveals the detailed packing pattern of SBA tetramers and the location of ligands in the microtube. As shown in Figure 3b, the intact tetrameric SBA serves as the building block of the microtube as designed. There is no significant change in conformation between the self-assembled tetramer in the microtube and the free tetramer in solution (Figure S11). Only a small conformational change around the substrate binding pocket was observed, which might be caused by the binding of **R3GN**.

SBA tetramers self-assemble into a microtube featuring a twisted helical structure. The reconstructed map revealed three smooth protofilaments winding around a hollow core in a left-handed fashion (Figure 3b, marked as red, yellow, and blue). Each protofilament exists as a periodic helical structure with a period of ∼19 nm. Each of the periodic structures consists of nine tetrameric SBAs (Figure 3c). The tetrameric SBA model fitted into the electron density map is shown in Figure 3d. The cross section of the structural model resolved the boundaries of the three protofilaments perpendicular to the tube axis (Figure 3e). The tubular structure encompasses a central and putative water-filled hole of ∼20 nm diameter, and the wall surrounding the hollow core is formed by a single layer of SBA tetramer of ∼4 nm thickness (Figure 3e). In short, the reconstructed model

DOI: 10.1021/jacs.5b11733
J. Am. Chem. Soc. 2016, 138, 1932−1937

explains well the data obtained from cryo-EM (Cryo-ET), AFM, and negative-stain EM.

Although the electron density of the designed ligands was clearly shown in the map, we were not able to build an accurate structural model of the ligands into the density map because of its limited resolution (Figure S12). Thus, we computationally modeled and positioned the ligand, **R3GN**, between adjacent tetrameric SBAs by combining the information on the atomic structures of previously designed ligand (Protein Databank (PDB) accession code: 4P9W), GalNAc (PDB accession code: 1SBE), and the 7.9 Å density map. Figure 4b zooms in on four

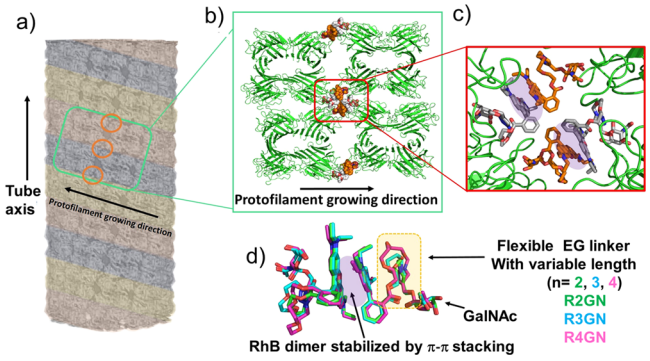

Figure 4. (a) Electron density map of a microtube as shown in Figure 3b. The three protofilaments are colored in translucent red, blue, and yellow. Four adjacent tetrameric SBAs, which belong to two neighboring protofilaments, were boxed in green. The location of **R3GN** pairs in the box is circled in orange. (b) Ribbon representation of four adjacent SBA tetramers is shown in green; four pairs of **R3GN** dimers are shown as spheres. (c) Close-up view of the atomic structure of two pairs of **R3GN**. Two $\pi-\pi$ interfaces are highlighted in light purple. SBA is shown in surface representation. The **R3GN** molecules are placed within the protein microtube considering the corresponding electron density and molecular simulation. (d) Flexible EG linker does not change the conformation and orientation of GalNAc and RhB. When overlaying the GalNAc-EG-RhB pair with different EG linkers (**R2GN** in green, **R3GN** in cyan, and **R4GN** in magenta), the corresponding RhB and GalNAc molecules nearly overlap, respectively.

adjacent SBA tetramers from two neighboring protofilaments, which are connected by four **R3GN** pairs. The formation of **R3GN** dimer mediates tetrameric SBA coming into the protofilament along its growing direction. Then, two neighboring SBAs in one protofilament are connected via two pairs of **R3GN**. According to the computational modeling, **R3GN** pairs only formed within each protofilament. Within each **R3GN** pair, the RhB module forms a dimer with its neighboring RhB (Figure 4c). For each **R3GN**, the GalNAc part settles in the sugar-binding pocket of SBA; the trizole group interacts with RhB by $\pi-\pi$ interaction (Figures S13 and S14). Given that the three designed ligands with different spacer lengths, **R3G**, **R2G**, and **R4G**, are capable of inducing the formation of microtubes with indistinguishable morphology, we then modeled and compared the dimeric structures of **R2GN**, **R3GN**, and **R4GN**, respectively. The results showed that the sugar pyranose rings as well as RhB in the three cases overlaid well (Figure 4d); the only difference was the length of the EG loop, which indicated that the effective length of the three ligands were the same despite the change in the spacer length of the EG linkers selected.

Kinetic and Thermodynamic Control of the Protein Microtube Formation. The formation mechanism of the protein microtube was studied by circular dichroism (CD) spectroscopy and cryo-EM. As shown in Figure S15, a strong negative peak appeared at around 583 nm in the CD spectra of the mixture of SBA and **R3GN**. According to our previous study,[32] this peak was associated with the J-type dimerization absorbance of RhB moiety in UV–vis spectrum, which normally appeared in CD spectrum as long as the RhB moiety entered a chiral environment, e.g., after its GalNAc part binding SBA. Thus, we monitor the microtube formation under different conditions by recording the peak intensity changes at 583 nm in CD spectrum. It was found that in the range of 3–10 °C, the speed of microtube formation was inversely correlated to the temperature (Figure 5a). Once the temper-

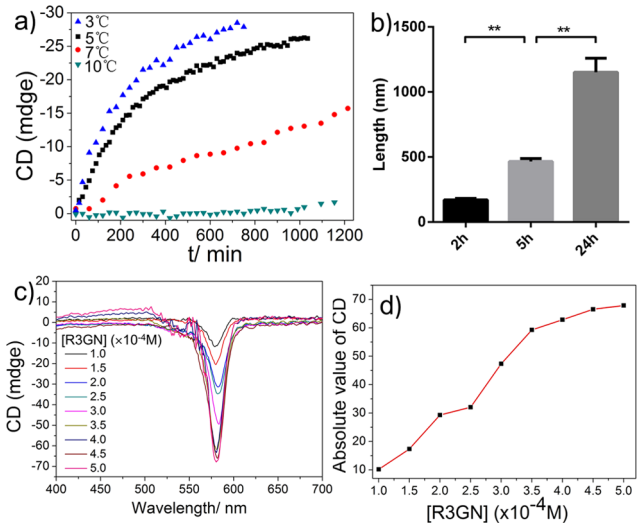

Figure 5. (a) CD spectra of SBA (0.2 mM) mixing with equivalent **R3GN** as a function of time at different temperature. (b) Tube length distribution with different incubation time of mixture of [**R3GN**] (0.2 mM) and SBA (0.2 mM) at 5 °C, calculated from Figure S16. (c) CD spectra of samples at different concentrations of **R3GN** with a fixed concentration of SBA (0.2 mM) at 5 °C. (d) Absolute CD value at 583 nm was plotted against the concentration of **R3GN**.

ature reached 10 °C, no change of the CD signal could be observed within 20 h. In addition, we found that the increase of the characteristic CD signal correlated well (Figure 5a at 5 °C) with the tube length (Figure 5b), revealed by cryo-EM results (Figure S16).

Protein microtubes were prepared under different ratios of [**R3GN**]/[SBA]. As shown in Figure 5c,d, when [**R3GN**] was increased from 0.1 to 0.5 mM, much larger negative peaks around 583 nm were observed. The plots of the maximum absolute CD value against [**R3GN**] suggested that the CD absorption went up with increase of [**R3GN**] when it was less than 3.5, whereas the CD increased speed was reduced when [**R3GN**] exceeded 3.5, which could be associated with the saturation of the sugar-binding sites on SBA. Moreover, as shown in Figure S17, with a higher ratio of ligand to protein, the tube length increased. To our surprise, even when the length of microtubes reached 10 μm scale, they were still stable in solution for at least a year, without any precipitation (Figure S18).

Reversibility of the Protein Microtube Controlled by Supramolecular Competition. Because the microtubule

DOI: 10.1021/jacs.5b11733
J. Am. Chem. Soc. 2016, 138, 1932–1937

formation is mediated by dual noncovalent interactions, we sought to control the process of the microtube formation and dissociation by modulating the interaction via supramolecular means. The control experiments showed that when the GalNAc moiety was replaced by mannopyranoside which does not bind to SBA, i.e., by using **R3M**, dimerization of RhB group could not be observed in CD spectrum confirming the key role of the specific interaction between GalNAc and SBA in this system (Figure S19a). Meanwhile, the role of the RhB dimerization was demonstrated by mixing the control sample **E3GN** with SBA (Figure S19a), which failed to generate microtube. Furthermore, after addition of 1 mM β-cyclodextrin (β-CD), a well-known host molecule to RhB,[35] to the suspension of microtubes formed by SBA and **R3GN** and incubation for 1 h, the CD signal (Figure S19b) disappeared, indicating the microtube dissociation. This was confirmed by cryo-EM observations (Figure S20a). The dissociation of microtubes was obviously caused by β-CD host incorporating RhB of **R3GN**. Interestingly, a subsequent addition of a competitive guest to the solution, 2 mM 1-adamantane hydrochloride (Ada), which binds β-CD[36] more strongly than RhB, induced the reformation of the protein microtubes (Figure S18b) after 48 h incubation. This resulted from the addition of Ada, which captured β-CD and released **R3GN**. In short, we demonstrated the reversible formation and dissociation of our protein microtubes by supramolecular means. This had not been reported for the protein tubular structures in literature, where their formation was driven by protein−protein interactions. The result implies the possibility of using the designed microtubes as controllable functional bionanomaterials.

Our data suggest that to some degree controlled supramolecular assembly of proteins can be realized via the synergy of SBA−sugar interaction and π−π stacking of RhB. More importantly, the kinetic and thermodynamic results indicate the pseudo-1D growth feature of the protein microtube. Considering the previous hypothesis that the twisting and growth of protofilament might be a crucial step of microtube formation, a possible mechanism is drawn in Figure 6. Here, on the basis of our previous study, we would like to emphasize that

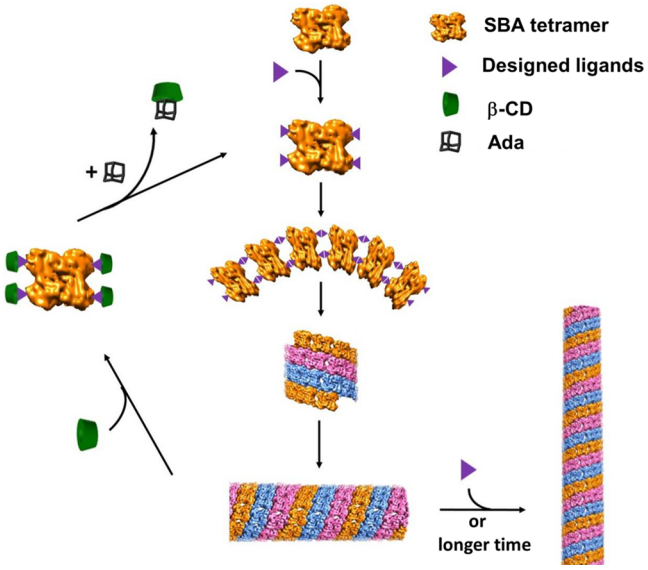

Figure 6. Possible mechanism of protein microtube formation and its reversibility to supramolecular interactions.

dimerization of RhB could not happen before Gal/GalNAc binds with SBA (Figure S21). The phenomenon ensures that this pseudo-1D growth happens directionally and accurately. Interestingly, this mechanism is quite different from the previously reported results, i.e., the protein microtube formation was driven by folding of 2D nanosheets,[19] which could not be as precise and accurate as the current pseudo-1D growth. Compared to 2D sheet folding, this pseudo-1D growth resembles more the supramolecular polymerization forming microtubules and filaments in nature.[18] Moreover, the current microtube formation can be controlled not only by temperature, incubation time, and ligand to protein ratio but also by supramolecular competition. These features make the supramolecular protein microtube quite unique to the other examples reported in literature and also render its microtubule-like character.

Immunological Function of the Protein Microtubes. Finally, immunological function of the microtube was evaluated. It is known that SBA itself is a Toll-like receptor (TLR) agonist and that TLRs are a class of proteins that play a key role in the innate immune system which usually is expressed on macrophages and dendritic cells. Meanwhile, GalNAc also has its own receptor on the surface of some immunological cells. To evaluate its immunological effect, the self-assembled microtubules was incubated with macrophage cell line RAW 267.4, and the released pro-immunological cytokine interleukin 4 (IL-4) by macrophages was used to evaluate their cellular state because the cell expresses acceptors to both of SBA and GalNAc on their surface. Meanwhile, SBA, **E3GN**, and their physical mixture (molar ratio = 1:1, SBA calculated as monomer) were also incubated with RAW 267.4 respectively as control. As shown in Figure 7, the microtubes

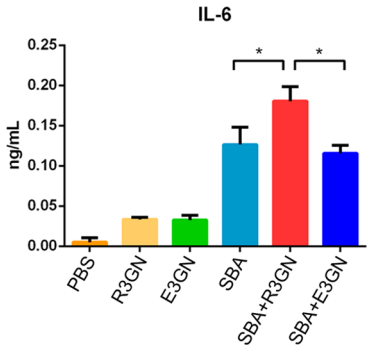

Figure 7. Cytokine release of macrophages induced by protein microtube formed by SBA and R3GN (red). Data was represented as means ± SEM. One-way ANOVA. *, $p < 0.05$.

induced the highest response of macrophages, compared to that of either of its two components or the physical mixture. The result is encouraging for further study on the immunological functions of the self-assembled microtubes based on proteins and sugar-containing ligand molecules.

■ CONCLUSIONS

In this work, a microtubule-like structure was constructed from a natural tetrameric protein and a series of designed hybrid ligands. The driving forces of this process are two supramolecular interactions, i.e., the molecular recognition between SBA and GalNAc/Gal and the π−π stacking of RhB. The structure of the microtube was determined at a resolution of 7.9

DOI: 10.1021/jacs.5b11733
J. Am. Chem. Soc. 2016, 138, 1932−1937

Å by cryo-EM and single-particle analysis. Together with computational modeling and biochemical data, we proposed a model for SBA microtube formation. To our knowledge, the designed microtube shown in this work features the first precise and reversible protein-microtubule-like structure reported in literature. Furthermore, the immunological study showed strong enhancement of immune response induced by SBA microtube compared to that induced by its tetrameric form, shedding light on the further design of microtube for immune adjuvant cargos and other applications.

■ ASSOCIATED CONTENT

Supporting Information

The Supporting Information is available free of charge on the ACS Publications website at DOI: 10.1021/jacs.5b11733.

Instruments and materials, synthesis of ligands, and additional data. (PDF)

■ AUTHOR INFORMATION

Corresponding Authors

*guosong@fudan.edu.cn

*liulab@sioc.ac.cn

Notes

The authors declare no competing financial interest.

■ ACKNOWLEDGMENTS

This work was supported by National Natural Science Foundation of China (Nos. 91227203, 51322306, 31470748, and GZ962), and the State High-Tech Development Plan (the "863 Program", Nos. 2015AA020907 and 2015AA020914) is acknowledged for their financial supports. We are grateful to the National Centre for Protein Science Shanghai (Electron Microscopy) for their instrumental support and technical assistance. Molecular graphics and analyses were performed with the UCSF Chimera package. Chimera is developed by the Resource for Biocomputing, Visualization, and Informatics at the University of California, San Francisco, California (supported by NIGMS P41-GM103311). The EM maps have been deposited in the Electron Microscopy Data Bank under accession code EMD-8065.

■ REFERENCES

(1) King, N. P.; Bale, J. B.; Sheffler, W.; McNamara, D. E.; Gonen, S.; Gonen, T.; Yeates, T. O.; Baker, D. *Nature* **2014**, *510*, 103−108.

(2) Fegan, A.; White, B.; Carlson, J. C.; Wagner, C. R. *Chem. Rev.* **2010**, *110*, 3315−3336.

(3) Salgado, E. N.; Radford, R. J.; Tezcan, F. A. *Acc. Chem. Res.* **2010**, *43*, 661−672.

(4) Oohora, K.; Onoda, A.; Hayashi, T. *Chem. Commun.* **2012**, *48*, 11714−11726.

(5) Luo, Q.; Dong, Z.; Hou, C.; Liu, J. *Chem. Commun.* **2014**, *50*, 9997−10007.

(6) Ueno, T. *Chem. - Eur. J.* **2013**, *19*, 9096−9102.

(7) Song, W. J.; Tezcan, F. A. *Science* **2014**, *346*, 1525−1528.

(8) He, N.; Lu, S.; Zhao, W.; Du, X.; Huang, S.; Wang, R. *Prog. Chem.* **2014**, *26*, 303−309. (in Chinese).

(9) Matsunaga, R.; Yanaka, S.; Nagatoishi, S.; Tsumoto, K. *Nat. Commun.* **2013**, *4*, 2111.

(10) Mejías, S. H.; Sot, B.; Guantes, R.; Cortajarena, A. L. *Nanoscale* **2014**, *6*, 10982−10988.

(11) Zhang, W.; Luo, Q.; Miao, L.; Hou, C.; Bai, Y.; Dong, Z.; Xu, J.; Liu, J. *Nanoscale* **2012**, *4*, 5847−5851.

(12) Staples, J. K.; Oshaben, K. M.; Horne, W. S. *Chem. Sci.* **2012**, *3*, 3387−3392.

(13) Sinclair, J. C.; Davies, K. M.; Vénien-Bryan, C.; Noble, M. E. *Nat. Nanotechnol.* **2011**, *6*, 558−562.

(14) Kitagishi, H.; Oohora, K.; Yamaguchi, H.; Sato, H.; Matsuo, T.; Harada, A.; Hayashi, T. S. *J. Am. Chem. Soc.* **2007**, *129*, 10326−10327.

(15) Sicard, D.; Cecioni, S.; Iazykov, M.; Chevolot, Y.; Matthews, S. E.; Praly, J. P.; Souteyrand, E.; Imberty, A.; Vidal, S.; Phaner-Goutorbe, M. *Chem. Commun.* **2011**, *47*, 9483−9485.

(16) Hou, C.; Li, J.; Zhao, L.; Zhang, W.; Luo, Q.; Dong, Z.; Xu, J.; Liu, J. *Angew. Chem., Int. Ed.* **2013**, *52*, 5590−5593.

(17) Jordan, M. A.; Wilson, L. *Nat. Rev. Cancer* **2004**, *4*, 253−265.

(18) Aida, T.; Meijer, E. W.; Stupp, S. I. *Science* **2012**, *335*, 813−817.

(19) Brodin, J. D.; Smith, S. J.; Carr, J. R.; Tezcan, F. A. *J. Am. Chem. Soc.* **2015**, *137*, 10468−10471.

(20) Brodin, J. D.; Ambroggio, X. I.; Tang, C.; Parent, K. N.; Baker, T. S.; Tezcan, F. A. *Nat. Chem.* **2012**, *4*, 375−382.

(21) Ghadiri, M. R.; Granja, J. R.; Milligan, R. A.; McRee, D. E.; Khazanovich. *Nature* **1993**, *366*, 324−327.

(22) Burgess, N. C.; Sharp, T. H.; Thomas, F.; Wood, C. W.; Thomson, A. R.; Zaccai, N. R.; Brady, R. L.; Serpell, L. C.; Woolfson, D. N. *J. Am. Chem. Soc.* **2015**, *137*, 10554−10562.

(23) Lo, P. K.; Altvater, F.; Sleiman, H. F. *J. Am. Chem. Soc.* **2010**, *132*, 10212−10214.

(24) Shafiei, F. *arXiv.org>Condensed Matter>Mesoscale and Nanoscale Physics*, **2015**, *1501*,01934.

(25) Huang, Z.; Kang, S. K.; Banno, M.; Yamaguchi, T.; Lee, D.; Seok, C.; Yashima, E.; Lee, M. *Science* **2012**, *337*, 1521−1526.

(26) Zhang, W.; Aida, T. *Science* **2012**, *337*, 1462−1463.

(27) Bong, D. T.; Clark, T. D.; Granja, J. R.; Ghadiri, M. R. *Angew. Chem., Int. Ed.* **2001**, *40*, 988−1011.

(28) Ballister, E. R.; Lai, A. H.; Zuckermann, R. N.; Cheng, Y.; Mougous, J. D. *Proc. Natl. Acad. Sci. U. S. A.* **2008**, *105*, 3733−3738.

(29) Miranda, F. F.; Iwasaki, K.; Akashi, S.; Sumitomo, K.; Kobayashi, M.; Yamashita, I.; Tame, J. R. H.; Heddle, J. G. *Small* **2009**, *5*, 2077−2084.

(30) Sendai, T.; Biswas, S.; Aida, T. *J. Am. Chem. Soc.* **2013**, *135*, 11509−11512.

(31) Song, W. J.; Sontz, P. A.; Ambroggio, X. I.; Tezcan, F. A. *Annu. Rev. Biophys.* **2014**, *43*, 409−431.

(32) Sakai, F.; Yang, G.; Weiss, M. S.; Liu, Y.; Chen, G.; Jiang, M. *Nat. Commun.* **2014**, *5*, 4634.

(33) Dessen, A.; Gupta, D.; Sabesan, S.; Brewer, C. F.; Sacchettini, J. C. *Biochemistry* **1995**, *34*, 4933−4942.

(34) Gupta, D.; Cho, M.; Cummings, R. D.; Brewer, C. F. *Biochemistry* **1996**, *35*, 15236−15243.

(35) Liu, Y.; Yang, Y. W.; Zhao, Y.; Li, L.; Zhang, H. Y.; Kang, S. Z. *J. Inclusion Phenom. Mol. Recognit. Chem.* **2003**, *47*, 155−160.

(36) Carrazana, J.; Jover, A.; Meijide, F.; Soto, V. H.; Vázquez Tato, J. *J. Phys. Chem. B* **2005**, *109*, 9719−9726.

DOI: 10.1021/jacs.5b11733
J. Am. Chem. Soc. 2016, 138, 1932−1937